Exploring the impact of semicore level electronic relaxation on polaron dynamics: An adiabatic *ab initio* study of $FePO_4$

Zi Wang and Kirk H. Bevan
Materials Engineering, McGill University, Montréal, Québec, H3A 0C5, Canada
(Received 9 October 2015; published 19 January 2016)

In the present work, we study the effects of the electronic relaxation of semicore levels on polaron activation energies and dynamics. Within the framework of adiabatic *ab initio* theory, we utilize both static transition state theory and molecular dynamics methods for an in-depth study of polaronic hopping in delithiated $LiFePO_4$ ($FePO_4$). Our results show that electronic relaxation of semicore states is significant in $FePO_4$, resulting in a lower activation barrier and kinetics that is one to two orders faster compared to the result of calculations that do not incorporate semicore states. In general, the results suggest that the relaxation of states far below the Fermi energy could dramatically impact the *ab initio* polaronic barrier estimates for many transition metal oxides and phosphates.

DOI: 10.1103/PhysRevB.93.024303

I. INTRODUCTION

In the rapidly evolving field of clean energy materials, many emerging and established materials exhibit polaronic behavior [1–5]. In particular, polaronic hopping conduction is understood to contribute to the low conductivity suffered by many of the transition metal (TM) oxides and phosphates typically utilized in batteries [6–11] and artificial photosynthesis [12]. Low conductivity often hampers the ability of these materials to harvest, store, or deliver energy. This usually occurs because d-shell electrons open a gap that localizes conduction electrons into small polaronic states [13,14]. In fact, there are many more materials with similar correlated mechanisms that produce localized carrier behavior, including ionic systems π-conjugated polymers [5,15], as well as electron transfer processes in ion-aqueous solutions [16]. In order to engineer and improve the electronic performance of this important class of materials, it is necessary to investigate and understand the fundamental mechanisms that determine their polaronic hopping behavior.

The simplest model of polaron hopping consists of a two-site model as sketched in Fig. 1 [17]. In this picture, an electron moves from one polaronic site to the next (e.g., two neighboring TM ions in an oxide/phosphate), by overcoming an activation energy E_a [17]. At the transition state, a hopping carrier is "shared between both sites" and if the coupling J is strong a gap opens up, the strength of which delineates adiabatic hopping from nonadiabatic hopping [17]. Now, it is usually assumed that the primary factors contributing to the hopping activation energy E_a arise form the nuclear reorganization of bonds between neighboring atoms during a polaronic transition [8–11]. For example, a TM oxide/phosphate atom possessing a small electron polaron will typically experience an expansion of bonds with neighboring oxygen atoms (sketched as a larger "expanded" red circle in Fig. 1) due to electron-electron repulsion, compared to those TM atoms lacking an extra electron (sketched as a smaller "contracted" blue circle Fig. 1). Likewise, the intermediate transition state is represented by a midsize magenta circle in Fig. 1, due to the midway extension of nuclear coordinates in this state. In the case of a hole polaron localized at a TM site, the process is described in an analogous fashion but with the situation reversed (i.e., there will be a contraction of TM-O bonds at the site of the hole polaron).

Such nuclear reorganization is, understandably, associated with the stretching of bonds and the corresponding relaxation of valence electron states. So logically one might assume that core electrons (both deep core and semicore as sketched in Fig. 1) play a negligible role in determining the polaron hopping barrier E_a [8–11]. From this follows the treatment of core electrons as "frozen," i.e., not relaxing during a hopping event. This would appear to be a fair approximation for well shielded deep-core levels [8–11]. However, the delineation is not so clear for semicore levels in transition metals (sketched in green in Fig. 1), even those situated many tens of eV below valence electrons [18]. Though core electrons do not participate in bonding, they can "electronically relax" during a hopping process and may contribute substantially to the overall hopping barrier E_a.

The impact of core-level relaxation is a subtle and important question, which goes back to the development of computational methods in quantum chemistry and condensed matter physics [18,19]. The most famous of these is Koopmans' theorem [and its density functional theory (DFT) variants] [20,21], which allows us to estimate the ionization and affinity energies of systems in terms of their single-particle eigenstates (ε). This is accomplished by assuming the orbitals are "frozen" during the ionization process. While this would appear to be a fair approximation when a charge state change occurs very rapidly relative to the time scale of electrons (e.g., optical excitations) [18,22], when ionization occurs on adiabatic (slow) time scales from the perspective of electrons, it is not clear which orbitals may be assumed to be "frozen" [18]. Small polarons provide an interesting framework to study the question of what orbitals can be viewed as "frozen," because hopping sites are often being ionized adiabatically/slowly (from the perspective of the much faster electrons) as an electron moves from one site to the next.

Due to computational limitations, in first-principles pseudopotential (PP) calculations on polaronic systems we often relax this "frozen orbital" assumption for valence electrons, but not for core electrons [8–11,22–25]. To shed light on this more general "slow ionization" problem in first-principles electronic structure theory [18–20], we address the question: what is the impact of semicore level relaxation upon the activation barrier of small polarons? As our model system we have chosen to study the delithiated form of $LiFePO_4$

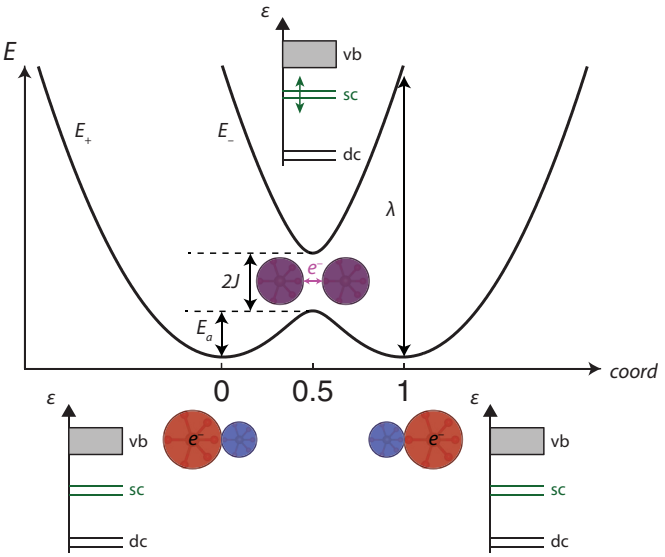

FIG. 1. Two-site electron polaron picture. Nuclear and electronic reorganization must occur to enable a polaron to reach the activation energy E_a, which represents the total energy (E) change that must be contributed by the system to move from a polaron localized on one atom (larger red circles) to another atom (smaller blue circles). At the intermediate transition state, the electron is shared by both sites (equally sized purple circles). During this transition, valence (vb), semicore (sc, in green), and deep-core (dc) levels (ε) may electronically reorganize/relax and contribute to E. Electronic coupling between polaronic sites is represented by J.

($FePO_4$, as shown in Fig. 2) [11], due to the known subtle interaction between the Fe d-shell and semicore states and the immense practical importance of this material in Li-ion batteries [1,11,23]. In this system, we show that semicore level relaxation can alter the estimated polaronic hopping rate by an

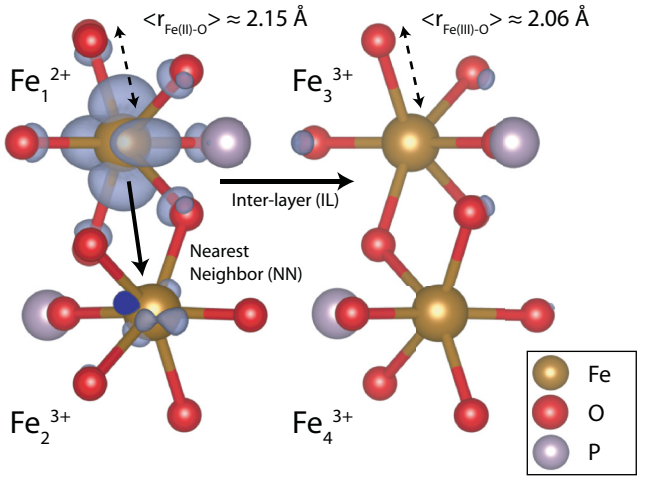

FIG. 2. The atomic structure of $FePO_4$. A polaron located on one site (labeled Fe_1), with an isosurface of the real space charge density shown in grey. Its nearest neighbor is labeled Fe_2, and its neighbor in the out of plane direction is labeled Fe_3. Consequently, we study both the common in-plane nearest-neighbor pathway (NN) as well as the closest interlayer pathway (IL). (Image generated with the VESTA software package [29].)

order of magnitude or more. While the focus of this study is on electron polarons in $FePO_4$, we find a similar effect for hole polarons in $LiFePO_4$ [26]. In general, it is expected that these results will have broad implications for first-principles polaronic hopping estimates in many TM compounds. The remainder of the paper is organized as follows: in Sec. II we outline the relevant concepts in polaron theory (Secs. II A and II B) followed by the computational details of this work (Sec. II C); then, we present our first-principles results in Sec. III (Secs. III A and III B); lastly, we discuss the general implications of our results in Sec. III C followed by a summary conclusion in Sec. IV.

II. METHOD

The physical properties of small polarons in solids closely resemble those of localized electrons on molecular sites, and as such polaronic theory borrows many concepts from molecular electron transfer (ET) theory (and vice versa) [13,27,28]. The reorganization energy (λ in Fig. 1) due to bond relaxation from the change in oxidation state can also be seen as similar to the molecular picture, where in this case it is the relaxation of TM-oxygen bond lengths on the TM site where the additional electron is localized. Small polaron hopping is therefore also analogous to ET theory, where the Franck-Condon principle requires that the electronic levels of the two sites are brought close enough together in order for hopping to occur, which can be accomplished by arranging the TM-oxygen shells to have the same bonding coordination (see Figs. 1 and 2). Below, we further outline these fundamental concepts and theoretical considerations in polaronic hopping in Sec. II A, followed by a detailed discussion of *ab initio* core relaxation and polaron hopping approaches in Sec. II B and an explanation of the computational method we have adopted in Sec. II C.

A. Two-site polaronic hopping model

The model Hamiltonian for a two-site polaronic system may be written as [17]

$$\mathcal{H} = \frac{M}{2}\left(v_1^2 + v_2^2\right) + \frac{M}{2}\omega^2\left(x_1^2 + x_2^2\right) + A(x_1 - x_2)(\hat{a}_1^\dagger\hat{a}_1 - \hat{a}_2^\dagger\hat{a}_2) + J(\hat{a}_1^\dagger\hat{a}_2 + \hat{a}_2^\dagger\hat{a}_1), \quad (1)$$

where M is the polaron effective mass, A is an electron-phonon coupling parameter, and J is the intersite coupling parameter. The velocities of the two sites are given as $v_{1,2}$ and the annihilation/creation operators as $\hat{a}_{1,2}/\hat{a}_{1,2}^\dagger$. The harmonic oscillation frequency in each polaronic well, sketched in Fig. 1, is defined as ω (usually it is regarded as an optical frequency) [17]. Looking only at positional differences $x = x_1 - x_2$ and ignoring center of mass $(x_1 + x_2)/2$ terms, this expression simplifies to

$$\mathcal{H} = \frac{M}{2}v^2 + \frac{M}{2}\omega^2 x^2 + Ax(\hat{a}_1^\dagger\hat{a}_1 - \hat{a}_2^\dagger\hat{a}_2) + J(\hat{a}_1^\dagger\hat{a}_2 + \hat{a}_2^\dagger\hat{a}_1), \quad (2)$$

with a single velocity v and reaction coordinate x for the system. Solving for the energies of this model Hamiltonian

then gives

$$E_{\pm}(x) = \frac{\omega^2 M}{4} x^2 \pm \sqrt{A^2 x^2 + J^2}, \tag{3}$$

which is shown schematically in Fig. 1. There are two energy levels separated by the coupling constant J, with E_- being the adiabatic ground-state energy and E_+ the excited diabatic energy level.

Importantly, within this two-site model the diabatic (or nonadiabatic) and adiabatic activation energies can be expressed in terms of the reorganization energy λ:

$$E_{\mathrm{a,dia}} \approx \frac{\lambda}{4}, \quad E_{\mathrm{a,ad}} \approx \frac{\lambda}{4} - J. \tag{4}$$

Furthermore, from the derivations shown in more detail in Ref. [17], there are three resulting characteristic polaron parameters, which can be utilized to understand how hopping should be treated in a given system:

$$\eta_1 = J/E_a \quad \text{(polaron size)}, \tag{5}$$

$$\eta_2 = \frac{J^2}{\hbar\omega\sqrt{E_a kT}} \quad \text{(adiabaticity)}, \tag{6}$$

$$\eta_3 = J^2/E_a kT \quad \text{(nearest neighbor)}, \tag{7}$$

where η_1, η_2, and η_3 describe, respectively, the polaron size, adiabaticity, and the validity of the nearest-neighbor approximation.

Most *ab initio* methods currently employed rely on the adiabatic approximation, i.e., the electrons always remain in the lowest possible energy levels during nuclear motion. In charge transfer processes, including small polaronic hopping in our case, this approximation might not always be valid. The hopping rate Γ derived from this two-site model is divided into adiabatic and diabatic regimes depending on the value of the adiabaticity parameter η_2 [17]

$$\Gamma = \frac{\omega}{2\pi} e^{-E_a/kT} \times \begin{cases} 1 & (\eta_2 > 1), \\ \pi^{3/2}\eta_2 & (\eta_2 \ll 1). \end{cases} \tag{8}$$

Importantly, this parameter allows one to determine the applicability of ground-state adiabatic DFT to a problem that is inherently diabatic. For $\eta_2 > 1$, we are in the adiabatic regime. If, however, $\eta_2 \ll 1$, the adiabatic approximation will no longer be valid. Either case of the resulting expression in Eq. (8) gives an exponential relationship between the hopping rate and the activation energy E_a. This energy E_a is the difference in total energy between the transition state and the ground states $E_a = E_{\mathrm{TST}} - E_{\mathrm{GS}}$ (as sketched in Fig. 1). Such total energies can be extracted from *ab initio* calculations, where E_{TST} is the total energy at the transition state and E_{GS} is the total energy at the ground state.

B. *Ab initio* approaches in modeling polaronic hopping

Within DFT, the total energy expression (from which we extract polaron activation energies) may be further divided into electronic and ionic terms:

$$E = \sum \varepsilon_i - \frac{1}{2} E_{\mathrm{H}} - \delta E_{\mathrm{xc}} + E_{\mathrm{ionic}}, \tag{9}$$

where the electronic contribution is composed of a summation over the electronic eigenstates (ε_i), less one-half the Hartree energy E_{H}, and an exchange-correlation (XC) correction (δE_{xc}) [19]. Moreover, within the local spin density approximation (LSDA) and general gradient approximation (GGA) XC frameworks, the techniques of pseudopotentials [30] and more recently projector augmented wave (PAW) [23] potentials are amongst the most popular and widely used methods to approximate the all-electron (AE) scheme accurately for a wide variety of atoms and systems. The central idea of these methods is to separate the electrons into an inner core and an outer valence shell, with the assumption that outside a certain core radius the tightly bound core electrons have no significant overlap with the valence electrons and can therefore be frozen within the potential. For most applications, this is an excellent approximation. However, there is no fundamental reason why core levels must always remain frozen and cannot provide significant corrections to the total energy as formulated by Eq. (9). For atoms such as transition metals where the valence d states are more strongly bound to the core, this approximation might not be sufficient and could result in significant discrepancies in energies (that is, core levels within $\sum \varepsilon_i$ and thereby E) [23,24]. Moreover, the inclusion of spin polarization leads to localized spin densities that may have subtle interactions with the core electron density.

For PP and PAW methods, one can construct a potential which treats semicore states as valence states [23,25]. This allows for the adiabatic relaxation of semicore states during hopping calculations at a slightly increased computational cost. For iron, in our model system of $FePO_4$, this means that we should place at least the $3p$ states and likely also $3s$ states in the "valence shell." Additionally, to fully capture polaron localization, it is necessarily to incorporate onsite TM electron-electron interactions (see Fig. 2). In this work, we have utilized the Hubbard DFT + U formalism [31], which leads to further localized d states and more spin interaction [6,7,32], further motivating the need to verify the accuracy of frozen core calculations by comparing them with the inclusion of semicore valence states. From hereon, we label the Fe $3d^6 4s^2$ results with Fe_{fc} and the Fe $3s^2 3p^6 3d^6 4s^2$ results with Fe_{sc} during the course of our study of $FePO_4$.

To calculate the activation barriers (E_a as shown in Fig. 1) between the polaronic sites from first-principles, one usually assumes a nearest-neighbor (NN) pathway and interpolates coordinates between the two endpoints as a good initial estimate [6,7,32], and might apply the climbing image nudged elastic band (CI-NEB) [7,33] method to further relax the pathway—hereafter simply abbreviated as the nudged elastic band (NEB) method. In most situations, this initial pathway estimate is well justified and results in a realistic barrier height, after relaxing this pathway using NEB. Additionally, it is assumed that hopping is adiabatic. In this work, we investigate in more detail where and why the adiabatic assumption is justified for our $FePO_4$ model system (as shown in Fig. 2). We do this by not only looking at the typical in-plane, nearest-neighbor (nn) pathway, but also by considering a hypothetical pathway between layers (interlayer). In this manner, we are able to study the validity of the adiabatic approximation on both pathways using a simple two-site polaronic transfer model [17,34] within the context of the general criteria given

by Eqs. (6) and (8) [27], and the impact of semicore level relaxation on the NEB computed polaron hopping barriers.

However, NEB calculations do not provide any information regarding the attempt frequency $\omega/2\pi$ [as expressed by Eq. (8)]. Molecular dynamics (MD) calculations, both analytical and quantum mechanical (*ab initio*, AIMD), are typically used to study dynamic processes such as surface diffusion [35,36] and more specifically ionic diffusion through battery materials [37,38]. In our model $FePO_4$ system, we use AIMD to study polaron dynamics, as polarons diffuse through the collective motion of its nearby atoms. The advantage of MD calculations is that it allows us to treat the system in a dynamic fashion while including the effects of thermal fluctuations, as well as extract both the activation energy and the hopping attempt frequency ($\omega/2\pi$) simultaneously through the Arrhenius relation,

$$\Gamma = \nu_0 \exp(-E_a/kT), \tag{10}$$

where $\nu_0 = \omega/2\pi$ is the frequency prefactor (hopping attempt frequency) and E_a is the activation energy. Similar work has been done previously on TiO_2 [2]. We can then relate these results to the barriers obtained from static (NEB) calculations, to both verify the static results and provide more detailed information on the hopping physics.

C. Computational approach

Calculations were done utilizing the GGA functional by Perdew, Burke, and Ernzerhof (PBE) [39] using projector augmented wave (PAW) [23] potentials as implemented in the Vienna *ab initio* simulation package (VASP) [40]. The on-site Hubbard term (U) was added to the functional (GGA + U) to incorporate the strong electron correlation in the Fe $3d$ orbitals and has been set to $U_{\text{eff}} = 4.3$ eV according to previous calculations [6]. Static calculations were done using $1 \times 2 \times 2$ supercells with an energy cutoff of 500 eV and a k-point grid such that energies were converged to within 1 meV per unit cell. The ionic positions and supercell dimensions are fully relaxed, with interatomic forces lower than 0.01 eV/Å. Ferromagnetic ordering was assumed throughout. For polaron calculations, an extra electron was added to the $FePO_4$ supercell with a compensating background charge to maintain charge neutrality, and ionic positions were subsequently relaxed to turn the electron into a localized polaron. To obtain a polaronic ground state from the intrinsic configuration, we must break the symmetry between the different sites. We employ an approach that approximates the polaronic effect by manually elongating each of the six Fe-O bonds by 5%. This ensures an efficient localization of the electron and fast subsequent structural relaxation to the ground state.

The Fe PAW potentials Fe_{fc} and Fe_{sc} used in this study have 8 and 16 valence electrons, respectively. Additionally, the potentials have different core radii (2.3 a.u. and 1.9 a.u., respectively). A smaller core radius leads to a potential that is "harder," i.e., it leads to more accurate results at the expense of requiring a larger basis set [23]. However, the on-site Hubbard term applies to a projected on-site density matrix that is defined only inside the PAW sphere [41,42]. A smaller core radius will therefore have a different on-site projection, and might lead to different results. To investigate this in more detail, we first note that the band gap in both $FePO_4$ and $LiFePO_4$ does not change significantly depending on which Fe potential was used (see Ref. [26]).

Additionally, we have performed all-electron (AE) calculations according to the APW + lo method as implemented within the WIEN2K software package [43]. Very briefly, the APW method separates the wave function into spherical harmonics inside the muffin-tin (MT) spheres and plane waves outside, with full relaxation of all core states. Within this method, DFT + U is similarly defined only inside the MT spheres. If we then take the MT sphere radii to be the same as the respective PAW core radii, we can separate the contribution of semicore states from possible artifacts arising from DFT + U implementation specifics, especially in the case of our Fe_{fc} results. That is, we can use an MT sphere radius of 2.3 a.u., and yet allow full relaxation of semicore states within the APL + lo method in a straightforward fashion without having to construct a specific PAW potential. We label AE results as $AE_{2.3}$ and $AE_{1.9}$, respectively, with the subscript number corresponding to the Fe MT sphere radius used (atomic units). Details of our WIEN2k calculations are provided in Ref. [26].

MD calculations were performed with an energy cutoff of 500 eV and Γ-point sampling. The Nosé-Hoover thermostat [44] was used to control the temperature in an NVT-ensemble. Multiple calculations were run at various temperatures for 20 ps per run with a time step of 1 fs. Initial conditions were set by adding a random velocity to each atom in an intrinsic supercell, distributed according to the Maxwell-Boltzmann statistics corresponding to the required temperature.

A small polaron exhibits two distinct characteristics: a distortion from the equilibrium in the bond lengths of the FeO_6 octahedron surrounding the Fe site denoted by $\Delta r(t)$, and a localization of the extra charge on the same Fe site denoted by $\Delta\rho(t)$. We call this polaron-induced effect the charge distortion field. A hopping event is defined as the movement of this charge distortion field from one Fe site to another. In other words, both $\Delta r(t)$ and $\Delta\rho(t)$ must move from one Fe site to another in order for it to be considered polaronic hopping. We take the correlation of the lattice distortion and the amount of localized charge, $\Delta\rho(t)\Delta r(t)$, to be our metric for polaronic motion. In similar spirit, we take a linearized average of FeO_6 octahedron bond lengths as our approximation for a generalized polaron coordinate Δr, and take the difference of these coordinates between two Fe sites Δr_1 and Δr_2 to be our NEB coordinates.

For our MD analysis, we record individual hopping times Δt_i for all such events, after which the average temperature-dependent hopping rate is calculated as the mean of the individual rates. We then plot these averaged rates as function of temperature, and extract the hopping barrier according to the Arrhenius equation of Eq. (10). This way, we can obtain both the activation energy and the prefactor (hopping attempt rate) from the same set of MD calculations. It should be noted that this method of hopping statistics is different from classical methods [35,36], where it is more common to calculate diffusivities from mean-square displacements of the system at the end of the run, for many runs. The current method takes each hopping event individually and thus exhibits a larger statistical variance, however, this is unavoidable due to the significant computational cost of running long *ab initio* MD simulations.

III. RESULTS

Before delving into detailed activation barrier (E_a) and rate (ω) calculations, let us start from the outset by addressing the question: is there any noticeable relaxation amongst semicore levels during the polaronic hopping process? To address this, we have fully relaxed the transition state barrier for a polaron hopping between two NN sites as sketched in Figs. 1 and 2, utilizing the NEB method with the inclusion of Fe $3s$ and $3p$ semicore sates (Fe_{sc}). Comparative transition state activation energies will be presented shortly, but let us first turn our attention to Fig. 3(a), which shows the projected density of states (PDOS) of the Fe_{sc} atomic orbitals in the intrinsic $FePO_4$ configuration (i.e., without a polaron present). As expected due to symmetry, all the Fe $3s$ states have the same energy. Similarly, there are three peaks for the identical $3p_x$, $3p_y$, and $3p_z$ states. They lie deep below E_F and therefore do not influence the bonding properties of the system. This is further elucidated by their real-space distribution [inset of Fig. 3(a)], showing that these semicore states are spatially confined to their respective Fe centers. The $3d$ states are part of the valence and conduction bands, and the band gap is 1.9 eV, which is in good agreement with earlier calculations [45].

Adding an electron in Fig. 3(b) leads to the formation and occupation of a polaronic state as shown by the sharp $3d$ peak at the Fermi energy. However, this also breaks the symmetry and lifts the degeneracy of the Fe $3s$ and $3p$ semicore states, separating them in energy. In other words, there is significant polaron induced electronic relaxation of the deeper lying states, an effect that would not be present if those states were kept frozen. Moreover, the electronic relaxation of the semicore states is pronounced when we move from the polaronic ground-state configuration "POL" in Fig. 3(b) to the polaronic transition state "TST" in Fig. 3(c) (e.g., coordinates 0 and 1 in Fig. 1, respectively), where the electronic levels undergo a nontrivial shift and splitting between their relative energies. While the bonding chemistry is accurately described by the polaronic state at E_F and surrounding $3d$ states (red in Fig. 3), the electronic relaxation of semicore states between the "POL" and "TST" configurations can lead to different total energies (and thereby activation energies E_a) depending on whether a semicore (Fe_{sc}) or frozen-core (Fe_{fc}) potential is used in the calculation as expressed by Eq. (9). A similar relaxation of semicore states was calculated in $LiFePO_4$ (provided in Ref. [26]).

In the subsequent sections, we investigate the effects of semicore relaxation by comparing results with an Fe_{fc} potential, which keeps the $3s$ and $3p$ states frozen, and a Fe_{sc} potential, which allows these semicore states to fully relax. It follows that there is a significant difference in polaron activation energies and dynamics depending on which potential is used. Our results show similar trends in both cases that dynamic barriers obtained from MD are comparable to static (NEB) barriers, and that non-NN hopping is significant. Using a basic two-site hopping model, we then show that only the NN pathway is within the adiabatic regime, validating both assumptions in the case of $FePO_4$. We argue that it is necessary to verify these conditions when modeling similar polaronic materials.

A. NEB

Figure 4 shows our calculated hopping barrier (E_a) for electron polarons in $FePO_4$, whose NN value in Fig. 4(a) for the Fe_{fc} case (blue triangles) is comparable to previously calculated results (see also Fig. 2) [6,7]. Figure 4(b) shows the calculated barrier for the non-NN interlayer (IL) pathway (see also Fig. 2). The energies for the Fe_{sc} study are shown as red squares.

Overall, in Fig. 4, we can clearly observe the energetic differences between the two potentials: using the Fe_{sc} potential leads to barriers that are roughly 100 meV lower than the barriers obtained with the Fe_{fc} potential. We attribute this discrepancy to the localized electron inducing additional electronic relaxation and spin interactions with lower lying semicore states on the Fe sites (as illustrated in Fig. 3). Moreover, we can compare the results with those obtained from AE calculations [26]. For the Fe_{fc} potential, the barrier is 142 meV compared to a barrier of 77 meV for the $AE_{2.3}$ calculation. The barrier for the Fe_{sc} potential is 52 meV, compared to the $AE_{1.9}$ barrier of 46 meV. The significant difference between the Fe_{fc} and the $AE_{2.3}$ barrier, combined with the smaller difference between Fe_{sc} and $AE_{1.9}$, underscores that semicore relaxation is the main cause of the lowering of the barrier. It is known that having semicore valence electrons leads to more accurate results for magnetic transition metals such as iron [23]. In the case of polaronic hopping barriers in $FePO_4$, this leads to a significant lowering of the barrier, and predicted room temperature mobilities that are one or even two orders of magnitudes above that when using the more common Fe_{fc} potential (as outlined in Table I and to be discussed shortly). A similar trend was computed in $LiFePO_4$, with the Fe_{fc} barrier at 257 meV and the Fe_{sc} barrier at 79 meV (see Ref. [26]). We argue that this might affect hopping barriers in other transition metal polaronic materials such as hematite and titanium dioxide in a similar fashion and recommend that energy calculations be done using potentials that incorporate semicore electrons in the valence states.

Additionally, an issue frequently encountered in magnetic systems is the existence of many local minima arising from the many different spin configurations that are locally favorable. Inclusion of the Hubbard U parameter lifts the orbital degeneracy and further exacerbates this issue, leading to configurations that are separated in energy on the order of hundreds of meV. This leads to self-consistent solutions that are highly sensitive to small variations in geometry, volume, and even numerical algorithms and mixing parameters [46]. Furthermore, these solutions are not guaranteed to have the lowest possible energy of that particular system [46]. In order to systematically improve convergence to the true polaronic ground state in transition state calculations such as those shown in Fig. 4, we have found it necessary to apply the U-ramping method proposed by Meredig *et al.* [46]. In brief, this involves calculating the ground at $U = 0$ eV, then gradually increasing the U parameter until we reach the desired value for U. At that point, it is more likely that the self-consistent solution has been nudged to the true ground state [46], increasing the confidence that our results are consistent. We found that ramping up U by 1 eV per iteration enabled us to consistently obtain accurate energies, especially for images near the transition state.

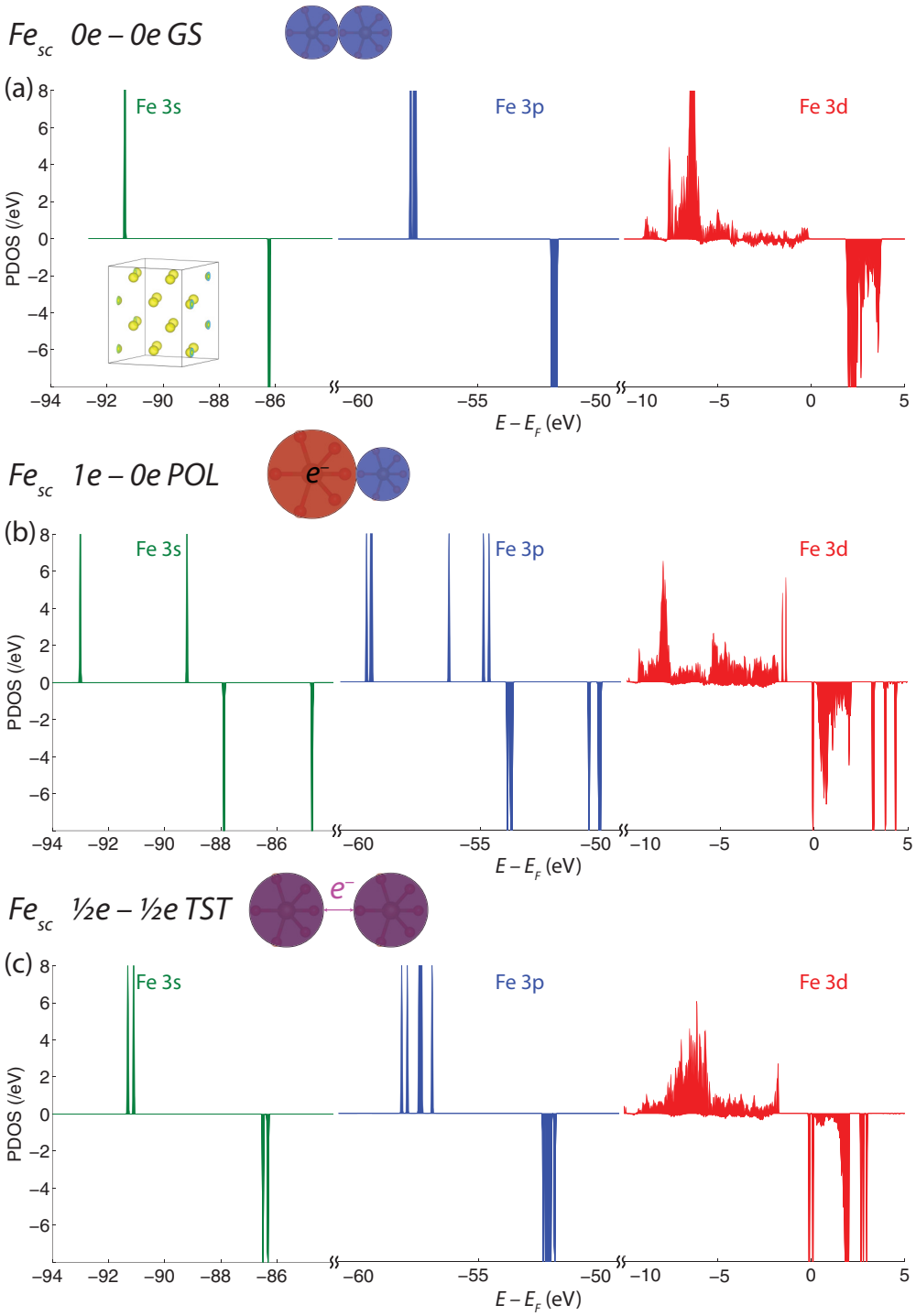

FIG. 3. Projected density of states (PDOS) for the two Fe atoms taking part in the electron transfer process for three relevant configurations represented by the schematic images of FeO_6 coordinations as introduced in Fig. 1. The PDOS for majority and minority spin are plotted on the positive and negative vertical axis, respectively. The semicore 3*s* (green peaks, left) and 3*p* (blue peaks, center) states lie deep below the Fermi energy, while the 3*d* (red curves, right) valence states contribute to the chemistry of the system. (a) PDOS of the intrinsic ground-state configuration ("GS") without additional electrons introduced. [(a), inset)] Real-space distribution of the Fe 3*s* semicore states. (b) PDOS of the polaronic ground state ("POL"), i.e., the electron is fully localized on one Fe site. (c) PDOS of the transition state ("TST"), where both Fe sites have similar coordination and share the additional electron.

Furthermore, it is commonly understood [6,7] that electronic transport in $FePO_4$/$LiFePO_4$ is primarily two-dimensional, staying within the plane due to Fe sites being separated by just O atoms in between (e.g., hopping between Fe_1 and Fe_2 in Fig. 1). The interlayer pathway has phosphate groups isolating the Fe sites, obstructing conductivity in the third dimension (e.g., hopping between Fe_1 and Fe_3 in Fig. 1). However, our calculations in Fig. 4(b) show that this IL

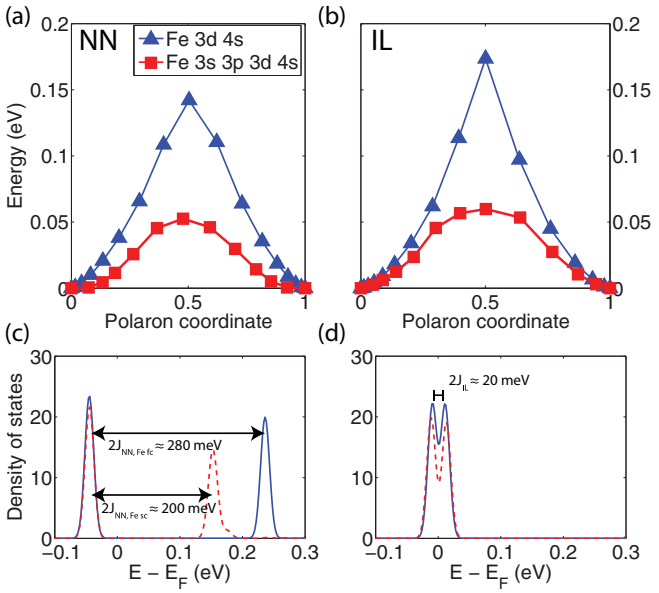

FIG. 4. Activation energies (a) and (b) calculated with the CI-NEB method [33] using both 8-valence $3d^6 4s^2$ (Fe_{fc} blue upright triangles) and 16-valence $3s^2 3p^6 3d^6 4s^2$ (Fe_{sc} red squares) Fe potentials, together with the level splitting at the transition state arising from the site coupling in (c) and (d), respectively. (a) and (c) nearest-neighbor (NN) barrier. (b) and (d) interlayer (IL) barrier.

pathway is energetically higher, but still within the range where hopping events could theoretically still be observed, in particular, for the low E_a estimate provided by the Fe_{sc} potential. To verify how realistic this predicted pathway is, we have conducted a more in-depth study of adiabaticity and the validity of the adiabatic approximation for both pathways.

Figures 4(c) and 4(d) show the Fe_{sc} and Fe_{fc} PDOS close to the Fermi energy E_F at the charge transfer transition state (polaron coordinate 0.5 in Figs. 1 and 4). In this state there is an equal probability of finding the electron on either site, and therefore a twofold degenerate polaronic state at E_F. Electronic coupling (J) then lifts this degeneracy and splits the two states into "bonding" and "antibonding" states. We take this separation between the bonding and antibonding states to be our approximation to the site coupling term J as $2J = E_{AB} - E_{bonding}$ as sketched in Fig. 1 and discussed in Sec. II A [47].

For the NN transition state $2J \simeq 200$ meV for Fe_{sc} and $2J \simeq 280$ meV for Fe_{fc}. This indicates that there is sufficient electronic coupling through the Fe-O-Fe bonds such that the NN transition may be regarded as adiabatic, as we shall evaluate shortly. For the interlayer transition state, however, there is a much weaker electronic coupling $2J_{inter} \simeq 20$ meV between the two sites regardless of the potential utilized, and both states remain at E_F. This can be attributed to the phosphate groups isolating the sites electronically (as shown in Fig. 2). Since the adiabaticity parameter η_2 as given by Eq. (6) depends strongly on J, we predict the interlayer transition to be highly diabatic and thus very unlikely to occur. It also implies that our results for the non-NN transition are unrealistic, as DFT is a ground-state theory and therefore inherently adiabatic—although time-dependent (TD) DFT should be able to capture such diabatic transitions.

To compute η_2 using Eq. (6) and fully evaluate adiabaticity, a frequency factor ω is required. As discussed in Sec. II A, this is usually taken as the optical phonon frequency of the system. Our approximation is to use the frequency prefactor of Eq. (10) obtained from MD calculations to estimate $\omega = 2\pi\nu_0$ as described in the next section [see also the discussion around Eqs. (8) and (10)]. Before detailing our MD results, let us briefly state the impact of the obtained frequencies on the adiabaticity parameter (η_2). For the nearest-neighbor pathway, we obtained $\eta_2 \simeq 0.35$ for Fe_{fc} and $\eta_2 \simeq 2.6$ for Fe_{sc}, concluding that the NN electron transfer process can be seen as reasonably adiabatic ($\eta_2 > 1$). However, for the interlayer pathway, $\eta_2 \simeq 0.002$ for Fe_{fc} and $\eta_2 \simeq 0.01$ for Fe_{sc}, respectively, indicating that this is a highly diabatic process. Therefore we argue that the nearest-neighbor pathway can be well approximated with common DFT methods, but that the results obtained for the interlayer pathway cannot be relied upon.

TABLE I. Barrier and frequency prefactors obtained from AIMD calculations. The advantage of using AIMD is that it enables us to calculate both barriers and prefactors simultaneously. Using these results, the diffusivities and mobilities were calculated at a temperature of 300 K. There is a ~20 meV discrepancy between MD and NEB computed barriers for both Fe_{sc} and Fe_{fc} potentials.

	Frozen core	Semicore
Nearest neighbor		
$E_{a,NEB}$ (meV)	142	52
$E_{a,MD}$ (meV)	151	28
ν_0 (10^{13} Hz)	14.75	5.26
D (cm^2/s)	6.41×10^{-4}	2.66×10^{-2}
μ ($cm^2/V\,s$)	0.03	1.03
Interlayer		
$E_{a,NEB}$ (meV)	174	59
$E_{a,MD}$ (meV)	143	26
ν_0 (10^{13} Hz)	14.19	4.92

B. Molecular dynamics

To compute the frequency prefactor $\nu_0 = \omega/2\pi$ and further verify the NEB computed activation barriers E_a, the hopping of electron polarons in $FePO_4$ was calculated in the temperature range of 300–500 K for Fe_{fc} and 143—300 K for Fe_{sc} calculations, with more hopping occurring at higher temperatures. Figure 5 shows a few characteristics of this hopping process (using the correlation methodology discussed in Sec. II C). While most of the iron sites and their oxygen bond lengths are in the Fe^{3+} ionic state ($\Delta\rho(t)\Delta r(t) \sim 0$), there is one site with high correlation, indicating that the polaron is currently located at that specific site. We can thus say that hopping occurs whenever another site takes over as the site with the highest polaron correlation.

As shown in Fig. 5, polaron transitions between sites are well distinguishable as transitions between curves with the highest charge-lattice correlation [$\Delta\rho(t)\Delta r(t)$]. The oscillations over time show the effects of adding thermal fluctuations, and hopping will take place whenever the random fluctuations

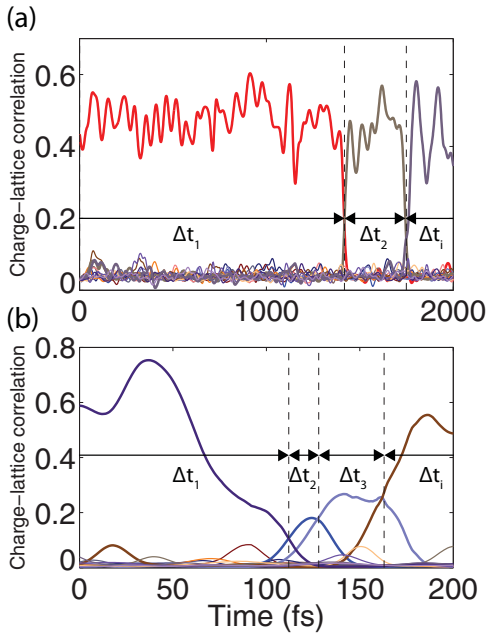

FIG. 5. Correlation analysis on a sample MD run. We calculate the average Fe-O_6 bond lengths of all 16 Fe sites scaled to unity, and multiply these values with their respective projected $3d$ electron occupations (also scaled to unity). The resulting charge-lattice correlation statistic should give a reasonable indication of the current polaron location.

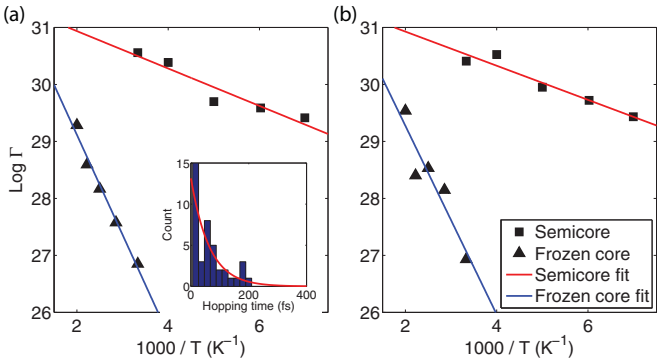

FIG. 6. Polaron AIMD hopping statistics. (a) Nearest-neighbor hopping. (b) Nearest interlayer hopping. Red line: linear fit of semicore calculations at $T = 143$, 166, 200, 250, and 300 K. Blue line: linear fit of frozen core calculations at $T = 300$, 350, 400, 450, and 500 K. Inset: exponential Poisson distribution of hopping times shown for one temperature point. The mean of this distribution was taken to be the mean hopping rate at that particular temperature. Similar statistics were done for each temperature point on these Arrhenius plots.

align to push the polaron over the energetic barrier, allowing both the distortion configuration and the extra charge to migrate to another location. We record the times of each such transition, and take the time between each transition Δt_i as their respective hopping time.

Theory [17] suggests that small polaron hopping exhibits a Markovian behavior, i.e., hopping events occur independently from each other at a constant average rate determined by the system temperature. We therefore expect our hopping events to be exponentially distributed (see inset of Fig. 6), and take the calculated average time between hopping events $\overline{\tau(T)}$ to be our typical rate $\overline{\nu(T)} = 1/\overline{\tau(T)}$. Calculating rates at different temperatures then allows us to view the relationship between temperature and average hopping rates, as shown in the Arrhenius plots of Fig. 6.

The numerical results are summarized in Table I. Diffusivities and mobilities were obtained from the typical relations [48]

$$D = \frac{l^2}{2d}\Gamma, \qquad \mu = \frac{e}{kT}D, \tag{11}$$

where $d = 2$ is the dimensionality of the system, e is the elementary charge, and $l \simeq 3.86$ Å is the nearest-neighbor distance between polaron sites (i.e., Fe atoms). Here we can see very clearly the impact of including semicore states. Not only does it change the barriers drastically, it also raises the hopping frequency accordingly due to these lower barriers. Whereas we can simulate $T = 500$ K within reasonable accuracy for Fe_{fc}, the average frequencies for Fe_{sc} are already nearing the numerical resolution of the 1 fs time step at $T = 300$ K. Our MD results are consistent with the predictions from our NEB calculations for the Fe_{fc} case, although the values for the Fe_{sc} MD results are consistently off by roughly 20 meV. This result casts into doubt the validity of the Markovian assumption, as hopping rates are so high [Fig. 5(b)] that the system might not have enough time to relax into its new polaron ground state before attempting another hop [17]. This might result in hops that are slightly correlated with each other inducing a slight memory effect, resulting in the lower calculated activation barrier. However, overall transition state theory (NEB) and the MD results agree fairly well.

Nevertheless, one could argue that there might be room to further improve the variance in the computed MD results, as exhibited within the inset of Fig. 6. However, we maintain that our results are statistically significant by noting that the barrier is exponentially related to these statistics. For example, a 20 meV increase in the MD computed barrier (in line with the NEB results in Fig. 4) would lead to a doubling of the mean and width of the distribution (in the inset of Fig. 6). Such a drastic change would not be achievable by sampling more points to reduce the variance.

C. Discussion

Overall, the results of our combined NEB and MD study (summarized in Table I) indicate a sizable ∼100 meV energy difference between Fe_{sc} and Fe_{fc} calculations of the polaronic hopping barrier E_a. We attribute this to the electronic relaxation of semicore states, including spin interactions, that are hard to capture within the frozen core approximation [as summarized by Eq. (9) and displayed in Fig. 3]. The activation barriers obtained with all-electron calculations further emphasize the effect of semicore relaxation in this material. A 100-meV discrepancy may be tolerable in some instances, however, in $FePO_4$ it leads to drastically different barriers and therefore a qualitative difference in diffusion analysis (as shown in Table I). With our lower barriers, the calculated diffusion constant and mobility are two orders of magnitude

higher than what was previously predicted. More practically, this opens up an interesting avenue of theoretical investigation in polaronic hopping during the charging and discharging of $LiFePO_4$ [1,11]. In particular, it indicates that the exceptionally low conductivity observed during $LiFePO_4$ intercalation might be due to correlated motion between polarons and Li ions. It also supports the notion that the rate-limiting factor in $LiFePO_4$ intercalation is the diffusion of Li^+ ions.

More generally, we argue that within the scope of polaronic materials and transition metal redox-type cathodes with strong spin-polarized *d* orbital correlation effects, the *p* (and perhaps also *s*) semicore states should always be included in the "valence" shell to capture and explore electronic relaxation and spin interactions. These interactions might even be significant for mid-to-late transition metals, which have larger *d* shells.

Furthermore, to evaluate adiabatic assumptions common in transition state theory based polaron hopping calculations, we have done an extensive molecular dynamics study on the free polaron hopping in $FePO_4$ to sample the available diffusion pathways in a dynamic fashion, incorporating both the typical nearest-neighbor pathway as well as the most likely nearest interlayer transition adiabatically. Our results show reasonable agreement within 10 meV compared with the NEB results for both the frozen core and semicore calculations. This remains within the precision of both NEB and MD methods. Though our adiabatic DFT calculations show a similarity in activation energies between the nearest-neighbor and nearest interlayer pathways, however, by looking at the interaction parameter *J* we have demonstrated that only the nearest-neighbor transition can be treated realistically within the adiabatic approximation typically inherent in Born-Oppenheimer based DFT. For the nearest interlayer transition, there is a phosphate group between the sites which lowers this *J* coupling to almost 0, indicating that such transitions are highly nonadiabatic and as such are far less likely to occur in reality. With this part of our study, we conclude that the nearest-neighbor assumption is well justified for $FePO_4$, but we argue that this condition should be verified for electronic transitions in all polaronic materials.

IV. SUMMARY AND CONCLUSION

In this work, we have looked at a few important concepts and *ab initio* specifics of polaronic behavior in TMOs using $FePO_4$ as our model system. Our *ab initio* computations were performed within the Hubbard DFT + *U* formalism, utilizing *U* ramping [46], applied to the conventional GGA DFT functional. In this model system, it was determined that interactions between spin-polarized *d* electrons and the semicore *p* and *s* electrons might significantly lower small polaronic hopping barrier estimates by up to ∼100 meV. While semicore levels do not participate in bonding, they can affect small polaron activation energies through electronic relaxation and spin interactions. As such, TMOs are interesting systems to study these effects due to the significant interaction between polaronic states and on-site core electrons. We argue that semicore relaxation might generally influence the properties of similar polaronic materials, and the impact of deep core-level interactions should thus be examined for these materials as well.

Furthermore, we have evaluated the adiabaticity of polaronic barriers in $FePO_4$. We have considered additional diffusion pathways, as well as sampled the stochastic nature of this system in a thermally fluctuating environment by means of AIMD. Our results have shown that, while there are indications of multiple pathways utilized by the system, only the nearest-neighbor pathway lies well within the adiabatic regime. Therefore our adiabatic transition state theory is insufficient in treating the other, nonadiabatic pathways accurately. Since polaronic hopping can be described as a series of electron transfer events, we argue that the assumption of adiabaticity should always be verified in similar polaronic materials. Moreover, we have shown that AIMD could be a useful tool in sampling pathways without prior assumptions, as well as obtaining the frequency prefactor without needing to resort to phonon calculations.

Lastly, on a more practical note, based on these lower polaron activation barrier results, we expect the rate-limiting factor in $LiFePO_4$ intercalation to be the hopping of Li^+ ions, having activation energies of more than four times that of free polarons [6–11]. Exploring correlated polaronic and Li^+ ion diffusion, in the context of semicore level relaxation, would be an interesting topic of future investigation.

ACKNOWLEDGMENTS

The authors acknowledge financial support from Natural Sciences and Engineering Research Council of Canada and computational support from Canada Foundation for Innovation, Compute Canada, and Calcul Québec. Z.W. acknowledges financial support from Mitacs of Canada, Hydro-Québec, and Fonds Québécois de la Recherche sur la Nature et les Technologies. Z.W. would like to thank Vladimir Timoshevskii, Bruno Rousseau, and Zimin Feng for insightful discussions on polaron physics.

[1] J. B. Goodenough and A. Manthiram, MRS Commun. **4**, 135 (2014).

[2] M. Setvin, C. Franchini, X. Hao, M. Schmid, A. Janotti, M. Kaltak, C. G. Van de Walle, G. Kresse, and U. Diebold, Phys. Rev. Lett. **113**, 086402 (2014).

[3] J. E. Katz, X. Zhang, K. Attenkofer, K. W. Chapman, C. Frandsen, P. Zarzycki, K. M. Rosso, R. W. Falcone, G. A. Waychunas, and B. Gilbert, Science **337**, 1200 (2012).

[4] P. Erhart, A. Klein, D. Åberg, and B. Sadigh, Phys. Rev. B **90**, 035204 (2014).

[5] C. Deibel, A. Baumann, and V. Dyakonov, Appl. Phys. Lett. **93**, 163303 (2008).

[6] T. Maxisch, F. Zhou, and G. Ceder, Phys. Rev. B **73**, 104301 (2006).

[7] G. K. P. Dathar, D. Sheppard, K. J. Stevenson, and G. Henkelman, Chem. Mater. **23**, 4032 (2011).

[8] V. Timoshevskii, Z. Feng, K. H. Bevan, J. Goodenough, and K. Zaghib, Appl. Phys. Lett. **103**, 073901 (2013).

[9] Z. Feng, V. Timoshevskii, A. Mauger, C. M. Julien, K. H. Bevan, and K. Zaghib, Phys. Rev. B **88**, 184302 (2013).

[10] Z. Feng, C. Kim, A. Vijh, M. Armand, K. H. Bevan, and K. Zaghib, J. Power Sources **272**, 518 (2014).

[11] V. Timoshevskii, Z. Feng, K. H. Bevan, and K. Zaghib, ACS Appl. Mater. Interfaces **7**, 18362 (2015).

[12] Y. Tachibana, L. Vayssieres, and J. R. Durrant, Nat. Photon. **6**, 511 (2012).

[13] I. G. Austin and N. F. Mott, Adv. Phys. **18**, 41 (1969).

[14] A. M. Stoneham, J. Gavartin, A. L. Shluger, A. V. Kimmel, D. M. Ramo, H. M. Rønnow, G. Aeppli, and C. Renner, J. Phys. Condens. Matter **19**, 255208 (2007).

[15] F. X. Morrissey, J. G. Mance, A. D. Van Pelt, and S. L. Dexheimer, J. Phys. Condens. Matter **25**, 144204 (2013).

[16] P. H.-L. Sit, M. Cococcioni, and N. Marzari, Phys. Rev. Lett. **97**, 028303 (2006).

[17] H. Böttger and V. V. Bryksin, *Hopping Conduction in Solids* (Akademie-Verlag, Berlin, 1985).

[18] F. Bechstedt, Phys. Status Solidi B **112**, 9 (1982).

[19] R. M. Martin, *Electronic Structure: Basic Theory and Practical Methods* (Cambridge University Press, Cambridge, 2004).

[20] A. Szabo and N. S. Ostlund, *Modern Quantum Chemistry: Introduction to Advanced Electronic Structure Theory* (Dover, New York, 1996).

[21] T. Koopmans, Physica **1**, 104 (1934).

[22] C.-G. Zhan, J. A. Nichols, and D. A. Dixon, J. Phys. Chem. A **107**, 4184 (2003).

[23] G. Kresse and D. Joubert, Phys. Rev. B **59**, 1758 (1999).

[24] J. Zhu, X. W. Wang, and S. G. Louie, Phys. Rev. B **45**, 8887 (1992).

[25] C. L. Reis, J. M. Pacheco, and J. L. Martins, Phys. Rev. B **68**, 155111 (2003).

[26] See Supplemental Material at http://link.aps.org/supplemental/10.1103/PhysRevB.93.024303 for Li_xFePO_4 band gaps, $LiFePO_4$ projected density of states, $LiFePO_4$ hole polaron activation energies, and WIEN2K calculation details.

[27] R. A. Marcus, J. Chem.l Phys. **24**, 966 (1956).

[28] A. L. Shluger and A. M. Stoneham, J. Phys. Condens. Matter **5**, 3049 (1993).

[29] K. Momma and F. Izumi, J. Appl. Cryst. **44**, 1272 (2001).

[30] S. G. Louie, S. Froyen, and M. L. Cohen, Phys. Rev. B **26**, 1738 (1982).

[31] V. I. Anisimov, J. Zaanen, and O. K. Andersen, Phys. Rev. B **44**, 943 (1991).

[32] Y. Sun, X. Lu, R. Xiao, H. Li, and X. Huang, Chem. Mater. **24**, 4693 (2012).

[33] G. Henkelman, B. P. Uberuaga, and H. Jónsson, J. Chem. Phys **113**, 9901 (2000).

[34] I. G. Lang and Y. A. Firsov, Sov. Phys. JETP **27** (1968).

[35] J. C. Tully, G. H. Gilmer, and M. Shugard, J. Chem. Phys **71**, 1630 (1979).

[36] K.-D. Shiang, J. Chem. Phys **99**, 9994 (1993).

[37] M. S. Islam, D. J. Driscoll, C. A. J. Fisher, and P. R. Slater, Chem. Mater. **17**, 5085 (2005).

[38] J. Yang and J. S. Tse, J. Phys. Chem. A **115**, 13045 (2011).

[39] J. P. Perdew, K. Burke, and M. Ernzerhof, Phys. Rev. Lett. **77**, 3865 (1996); **78**, 1396 (1997).

[40] G. Kresse and J. Hafner, Phys. Rev. B **47**, 558 (1993); **49**, 14251 (1994); G. Kresse and J. Furthmüller, Comput. Mater. Sci. **6**, 15 (1996); Phys. Rev. B **54**, 11169 (1996).

[41] O. Bengone, M. Alouani, P. Blöchl, and J. Hugel, Phys. Rev. B **62**, 16392 (2000).

[42] A. Rohrbach, J. Hafner, and G. Kresse, J. Phys.: Condense. Matter **15**, 979 (2003).

[43] P. Blaha, K. Schwarz, G. Madsen, D. Kvasnicka and J. Luitz, *WIEN2k, An Augmented Plane Wave + Local Orbitals Program for Calculating Crystal Properties* (Karlheinz Schwarz, Techn. Universität Wien, Austria, 2001).

[44] S. Nosé, J. Chem. Phys **81**, 511 (1984).

[45] F. Zhou, K. Kang, T. Maxisch, G. Ceder, and D. Morgan, Solid State Commun. **132**, 181 (2004).

[46] B. Meredig, A. Thompson, H. A. Hansen, C. Wolverton, and A. van de Walle, Phys. Rev. B **82**, 195128 (2010).

[47] N. Adelstein, J. B. Neaton, M. Asta, and L. C. De Jonghe, Phys. Rev. B **89**, 245115 (2014).

[48] G. Antczak and G. Ehrlich, *Surface Diffusion: Metals, Metal Atoms, and Clusters* (Cambridge University Press, Cambridge, 2010).